Composites Part C: Open Access 8 (2022) 100267

Contents lists available at ScienceDirect

Composites Part C: Open Access

journal homepage: www.elsevier.com/locate/composites-part-c-open-access

An experimental damage tolerance investigation of CFRP composites on a substructural level

Raffael Bogenfeld *, Christopher Gorsky, Tobias Wille

German Aerospace Center, Institute of Composite Structures and Adaptive Systems, Lilienthalplatz 7, Germany, Braunschweig, 38108, Germany

ARTICLE INFO

Keywords:
Damage tolerance
Fatigue
Delamination
Damage growth
Structural test
Aircraft design

ABSTRACT

The damage tolerance (DT) allowables for the design of a composite structure are typically determined through experiments on the coupon level. The present study examines the transferability of the DT behavior from the coupon level to a structural level. For that purpose, a DT critical panel with two stiffeners was designed and tested. In one quasi-static and two cyclic compression after impact tests, the damage evolution behavior was studied and compared with results achieved on the coupon level. Similar phenomena were found on both scales: a long interval of load cycles, without any detectable damage evolution is succeeded by the sudden propagation of the delamination and the fiber fracture. Afterward, the ultimate failure occurs within few load cycles. Even though the stiffened panel offers a significant possibility to transfer load from the damaged skin, a significant damage stabilization could not be achieved. The no-growth interval was found to be shorter on the structural scale, however, an analytical DT analysis suggests the different damage size as the most likely cause. However, it was found that the stiffeners slow down the damage propagation. Eventually, the study confirms the no-growth design approach as the preferred method to account for the DT of stiffened, compression-loaded composite structures.

1. Introduction

The structural integrity is vital to any transport aircraft. Any structural damage possibly occurring during the service life must not result in catastrophic failure. The state of the art to comply with the need to maintain the structural integrity is damage tolerance [1]. Due to manufacturing defects or external influence like impact threat, damage cannot be completely avoided in aircraft structures [2]. DT means taking into account this expected damage during the design. The design has to ensure a sufficient residual strength of the damaged structure over a specific design interval.

The typical design and analysis procedures for a damage-tolerant design are well-established for metallic structures, as provided for example in the structural analysis handbook (HSB) [3]. The damage, in form of a through thickness crack, can be considered to grow slowly and stably for a long interval and elementary fracture mechanical methods permit a sufficiently accurate prediction of the propagation. With regard to structures made of composite laminates, the damage-tolerant design is particularly challenging, due to "a multiplicity of failure modes", as described by Baker et al. in 1985 [4]. Nonetheless, also composites have to withstand the expected structural damage. According to Newaz and Sierakowski, composite structures have to "equal or exceed" [5] the safety standards of a conventional metal structure. Therefore, the public authorities define specific permissible methods to account for the DT of composites [6–8]. Briefly summarized, there are three admissible concepts which can be applied to approve the DT, slow growth, arrested growth and no-growth. Among these admissible concepts, a strict no-growth approach currently seems to be the only viable method to cope with delamination [9,10]. In practical application, the no-growth policy is realized through strain allowables, which may never be exceeded [11,12]. As outlined by Dienel et al. [13], aircraft manufacturers determine DT allowables "based on extensive experimental campaigns". This determination procedure is based on residual strength tests after impact [14,15]. To account for the operational load and a possible further strength decrease, residual strength testing after cyclic loading is additionally required [16], as demanded in the design guidelines (cf. AC 20-107B [6]). Due to the limited detectability of delamination through the visual inspection procedures [17], the design interval for barely visible impact damage (BVID) derives from the structural service life. Only special detailed inspection methods [18] or a structural health monitoring systems [19,20] would offer the possibilities to reduce the design-critical interval even for non-visible damage.

The mechanical behavior of impact-damaged composites under cyclic compression load is already well described in the literature.

* Corresponding author.
E-mail address: raffael.bogenfeld@dlr.de (R. Bogenfeld).

https://doi.org/10.1016/j.jcomc.2022.100267
Received 16 March 2022; Received in revised form 12 April 2022; Accepted 16 April 2022
Available online 25 April 2022

An overview is presented in the review by Nettles et al. [21]. In 24 considered studies, hardly any delamination growth was observed before the ultimate failure. If any growth was detected, it happened at high load levels and close to the ultimate collapse [22–25]. Only in some distinct cases, a significant period of delamination growth before the collapse is reported [9,11,26,27]. Likewise, a recent compression fatigue after impact (CFAI) investigation by Bogenfeld and Gorsky did not reveal significant damage growth before the ultimate failure [16]. However, another review by Molent and Haddad points out that there are various experimental damage growth studies from the literature [28] for different loading conditions. They conclude, that there are sufficient examples in the literature where a slow and stable damage growth behavior was proven to occur systematically.

Nonetheless, most available studies in the literature are bound to the coupon level, typically through a compression after impact (CAI) standard test [29–31] or a comparable coupon compression specimen. DT testing on the structural level is cumbersome, expensive, and can merely be conducted at an early stage of the design phase. However, various differences between a coupon and an actual stiffened structure possibly affect the DT behavior. A major factor of positive influence is the capability to transfer load on the structural level: the delamination on a coupon encompasses nearly the entire specimen width and does not offer an alternative load path, a BVID in a real composite structure is small in relation to the load-sustaining cross section and stiffening elements act as alternative load paths.

In contrast to that, there are also reasons to assume a less stable crack propagation on the structural level. According to the size effect described by Bažant [32,33], a large, damaged structure will failure earlier than a similarly-damaged, small structure.

Only few experimental studies on a larger scale exist. In 2018, Soto et al. [34] published quasi-static DT tests of stiffened panels, which exhibited an impact-driven strength decrease of more than 40 %. The ultimate failure occurred by fiber fracture in the skin across the entire specimen width. Furthermore, Tan et al. published experimental studies about the influence of damage on T-stiffened panels. Their results show a slight influence on the buckling load and a major decrease of the quasi-static failure load [35,36]. The studies of Soto et al. and Tan et al. confirm the relevance of BVID to the residual strength on a structural level.

However, there are hardly any published experimental studies dealing with impact-damaged, stiffened panels under fatigue loading. One study addressing this particular scenario is the work of Feng et al. [37]. They investigated the effect of fatigue loading to impact-damaged panels under cyclic and quasi-static loading. The CAI strength knock-down of 10 % increased to a 15 % knock-down after the cyclic loading. Nevertheless, the there were changes in the impact damage throughout the cyclic loading. This lack of any visible damage propagation raises the question how the DT failure under cyclic load would occur. The possible effects of stable and unstable damage propagation, stabilization through load transfer, and the endurance limit are still unanswered questions. In particular, the damage evolution behavior on the structural level has to be analyzed in the context of the known well-known effects on the coupon level.

In this work, we present an experimental investigation of three stiffened panels under quasi-static and cyclic compression load. Based on the laminate configuration of a previous series of coupon tests [16], the panel was designed for DT to be the critical failure mode. The panel tests are supplemented by test results from the referenced study which represents the corresponding coupon CCAI investigation. The effects driving the damage evolution and the ultimate failure are analyzed and compared on both scales with regard to the DT design allowable derived on the coupon level and its validity on a sub-structural scale.

2. Specimen configuration

The present investigation builds on a previously conducted series of quasi-static and cyclic compression after impact (CAI) tests [16]. The specimens in this reference study were made of carbon fiber reinforced plastic (CFRP) laminate and coupons according to the CAI standards by ASTM [30,31] or AITM [29]. To ensure the comparability of the panel test results with the available coupon test results, panel specimens of the same laminate as in the coupon tests are required. Nonetheless, there is no test standard available, defining an appropriate specimen or test setup. The panel design has to fulfill various requirements resulting from the study's purpose and the available test equipment. The crucial aim is to draw valid conclusions about the DT on a structural level. Hence, the panel has to represent a stiffened structure. Thus, there is a need for at least one alternative load path in addition to the skin laminate. As a consequence, the panel has to possess at least one stiffener bay, and thus, two stiffeners. Moreover, the panel shall be kept as simple as possible. Thus, ordinary stiffening elements with a T-profile shall be used. To ensure the comparability of the panel and coupon tests, the skin laminate of the panel shall be equal to the quasi-isotropic coupon laminate. This configuration of a stiffened panel with two T-stiffeners, as depicted in Fig. 1, is the baseline for the panel design. This panel configuration is comparable to the specimen used in the test campaign of Soto et al. [34]

For this two-stiffener configuration, the geometry parameters were defined to avoid stability failure and to meet the force capability range of the test machine. These parameters are the width, the length of the skin as well as size and the distance of the T-stiffeners. All relevant geometrical parameters of the panel configuration are shown in the sketch in Fig. 2. Both, the skin and the stiffeners are designed with a quasi-isotropic layup. The skin laminate with a thickness of 4 mm, the T-stiffeners with a thickness of 3 mm in one half. Hence, the stiffening ratio according to the structural analysis manual HSB section 63600 [3] calculates from the ratio of the stiffener cross section and the total cross section according to Eq. (1). The ratio for the defined panel is $\mu = 0.43$, neglecting the delta fillets in the stiffeners.

$$\mu = \frac{A_{stiff}}{A_{skin} + A_{stiff}} \tag{1}$$

The readily manufactured panel has to be embedded in resin blocks to be fixed in the machine. These blocks embed the panel skin and the stiffeners in their entire width and on a length of 60 mm, leaving a free panel length of $l_{free} = l_{total} - 2 \times 60$ mm. The panel length influences mainly the stability behavior. As stability failure shall be avoided, the free length has to be minimized. This results in the value of $l_{free} = 200$ mm and $l_{total} = 320$ mm.

All components were manufactured of an M21e/IMA prepreg material with a ply thickness of 0.127 mm. The skin and the stiffeners were cured on aluminum molds in separate autoclave processes. Due to the availability of the tooling, the skin was manufactured with a curvature of the radius 2075 mm. This curvature is compensated by the spring-in effect resulting in an angle slightly below 90° between the stiffener foot and the stiffener web. The delta fillet in the stiffener edge is manufactured of rolled unidirectional material and included during the stiffener manufacturing. The skin and stiffeners were bonded in another autoclave process. The components were joint through secondary bonding, using the adhesive film is FM300 K0.05 [38]. This adhesive has a high fracture toughness [39–41] exceeding the toughness of the ply interfaces in an M21e prepreg material [42].

The influence of the curvature was studied through numerical buckling analysis of the panel configuration. This pre-study revealed no relevant effect of the curvature to the global stability or the strength of the panel. Thus, we can assume that the curvature is hardly relevant to the DT behavior of the panel.

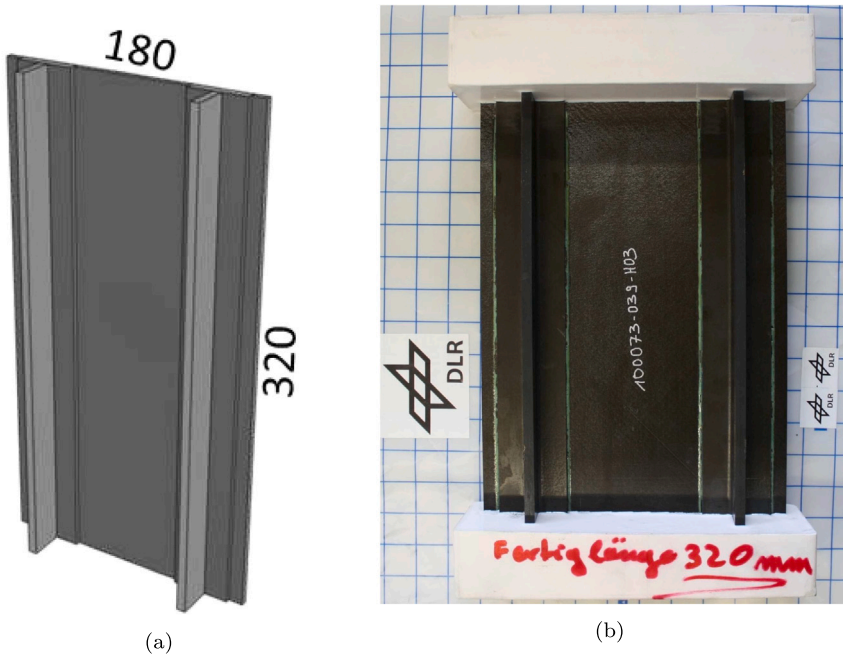

Fig. 1. 3D model of the panel configuration (a) and the manufactured specimen including the resin blocks on both ends (b).

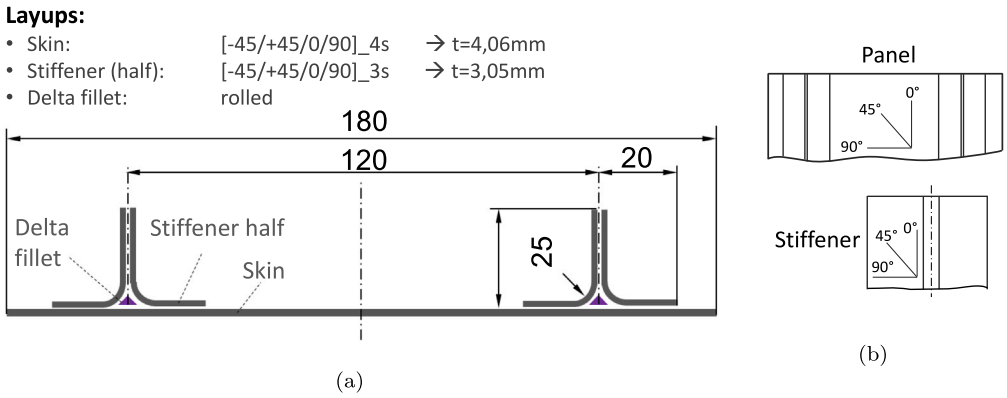

Fig. 2. Technical drawing and layups of the test panel with its final geometry parameters (a) and the coordinate systems for the layup (b).

3. Procedures of the impact and compression tests

The readily prepared panels were first impacted and afterward mounted into the test machine for the compression tests. The respective procedures were defined analogously to the CCAI tests on the coupon level [16]. In this section, we describe the tests in three parts: the impact, the quasi-static compression test, and the cyclic compression test.

3.1. Impact test

First, all three panels were subjected to a centric impact on the skin laminate. The impact was applied through a gas gun as shown in the Fig. 3. The gun was equipped with a hemispherical 16 mm impactor tip and an impactor mass of 0.835 kg. Furthermore, the gas gun has a displacement sensor measuring the impactor position with a sampling frequency of 50 kHz. A direct measurement of the contact force between the impactor and the specimen is not covered. However, the second time derivative of the displacement permits to calculate the acceleration history and thus, to calculate the contact force history. To obtain a meaningful result, the noise has to be removed from the data. As described by Gliszczinski et al. [43], a suitable curve can be obtained through a finite impulse response filter for the displacement history and its first derivative.

The skin laminate of the panels equaling that of the CAI standard specimens is a reason to assume a qualitatively similar damage behavior in both cases. However, the different stiffness toward out-of-plane indentation requires a different energy level to cause a similar damage size on both scale. For that reason, the impact response measured during the coupon experiments was scaled to panel impact in order to achieve an equivalent damage size. This scaling was conducted through the analytical scaling method of Bogenfeld et al. [44,45]. Under the basic requirement of similar laminates on both scales, this method permits one to transfer a known impact response to an unknown target case. A valid scaling result can only be achieved if the damage evolves qualitatively similar on both scales. The quantitative differences due to different boundary conditions are solved through the scaling of the impact energy. This scaling procedure resulted in a nominal impact energy of 42 J on the panel skin to equal the damage of the 35 J coupon impacts. After the impact, the entire impact damage of each panel was characterized through an ultrasonic D-scan in an immersion tank.

Fig. 3. Gas gun for the impact tests.

3.2. Compression test

The following compression tests were conducted on the buckling test facility of the DLR Institute of Composite Structures and Adaptive Systems. The buckling facility is suitable for testing panels as well as cylindrical shells and described in detail for example by Wilckens et al. [46] or by Khakimova et al. [47]. Fig. 4 shows the setup of the buckling test facility for the panel tests for the experiments of the present study. The machine is equipped with three force transducers arranged in parallel. Hence, the force applied to the specimen equals the sum of the three individual measured force values. To measure the displacement, an external displacement transducer measures the distance between the upper and the lower specimen fixtures. Thus, the measured displacement corresponds to the deformation of the entire panel including the resin blocks for the load introduction.

The first compression test was a quasi-static collapse test with the panel P66. This test serves as a reference to obtain the ultimate residual strength F_{ult}, which was determined as 315 kN.

The other two panels, P67 and P68, were subjected to cyclic compression load. A load level of 80 % was chosen relatively to F_{ult} which resulted in a failure between 5000 and 12 000 load cycles according to the CCAI coupon experiments. This load level corresponds to a maximum compression load of 252 kN.

The cyclic tests were conducted with a closed-loop force control. The absolute minimum force is defined through the load ratio $R = 10$. In the beginning of the test the loading frequency is 0.7 Hz. As soon as delamination growth was detected, the test was continued with the reduced frequency of 0.3 Hz to facilitate interrupting the test in case of further damage propagation.

The first cycle of each test was always conducted with a quasi-static load to be able to conduct a DIC measurement and to measure a high-sampled force response. Furthermore, after predefined intervals of load cycles or after acoustic/visible evidence of damage propagation, the test was interrupted. Before continuing the cyclic test, an ultrasonic scan through mountable ultrasonic transducer was conducted (cf. Fig. 5) and a photo of the surface damage was taken. If applicable, also a quasi-static test cycle with DIC measurement was conducted. The recorded data in form of the history of the ultrasonic scans, the surface photos, and the DIC measurements are depicted in the Appendix in the Figs. A.16, A.17, and A.18, respectively.

The cyclic test of the panel P67 was conducted with the above-described configuration until the ultimate failure under cyclic load. For the test of the panel P68, the test was slightly modified. After the ultrasonic scan evidently showed that the delamination grew, the control loop was switched to displacement control. Hence, a further damage propagation reduced the load as the stiffness of the sample decreased. This modification shall permit investigating the possibility to slow down the damage propagation in a stiffened composite structure.

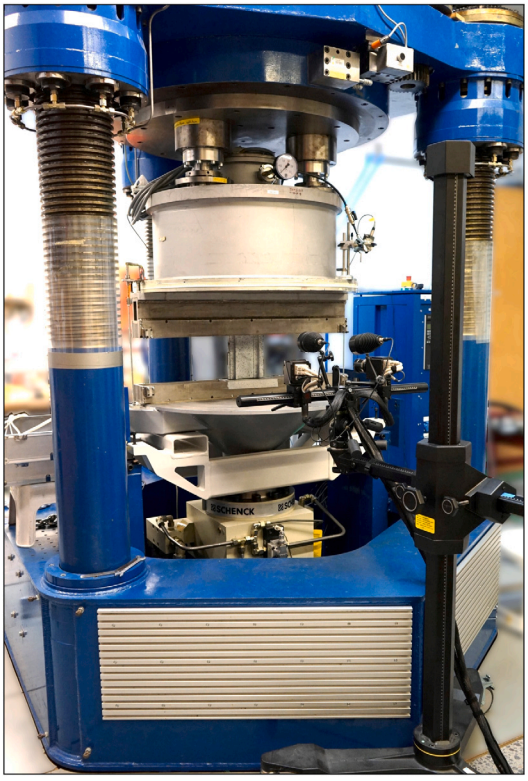

Fig. 4. Test setup for the panel compression tests in the DLR buckling test facility.

4. Results and discussion

4.1. Impact damage

Even though, the impact tests in this study are not the primary subject of the investigation, the impact damage is the driving initial parameter for the DT evaluation. Hence, the characteristics of the impact damage and their similarity between the three panels have to be analyzed to understand the DT results observed in the following compression tests.

The Table 1 provides in the first data row the actual impact energy for each individual panel. Due to the gas gun characteristics, there is a certain tolerance in the impact energy. Nonetheless, the impact energy of all three panels differs by less than 3 %. The impactor mass is a constant value for each impact. The maximum contact force, the contact duration, and the energy absorption derive from the force histories which are shown in Fig. 7. Only the maximum contact force exhibits notable differences between the three impacts. However, the force maximum is an inaccurate value in this case. The reason for this is the required filtering during the calculation of the force history from the displacement measurement (cf. 3). Nevertheless, the similarity of the force–displacement curves in Fig. 7 confirms the reproducibility of the impact test.

With regard to the damage, a qualitatively similar pattern occurred in all three cases, as the ultrasonic scan in Fig. 6 shows (Also, in Fig. A.16 of the Appendix the impact damage is shown for n=0). The centric damage at the impact location is dominated by large delaminations close to the middle layers of the laminate. As the detected delaminations in other interfaces are much smaller, these large delaminations in the middle dominate the projected delamination area. In addition, the visible damage on the impact side is shown in Fig. A.17. Inter-fiber fracture in the topmost plies is visible as straight cracks in ±45° directions. Furthermore, a jagged crack was observed in the

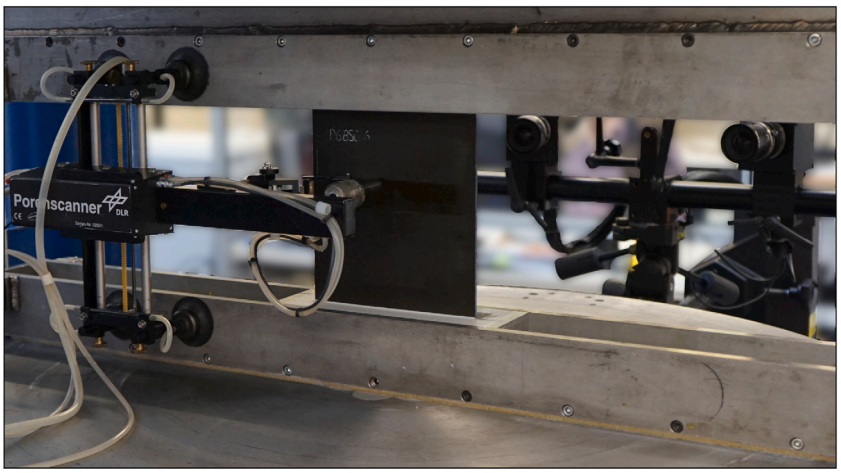

Fig. 5. Ultrasonic scan of the panel mounted in the testing machine.

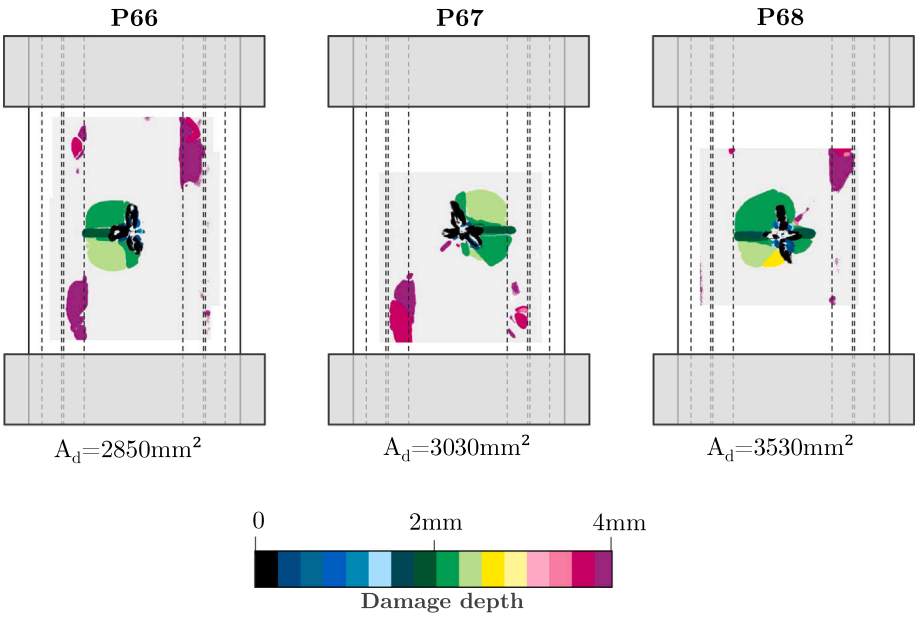

Fig. 6. Ultrasonic D-Scan results of each panel with its initial impact damage.

±90° direction. Due to the stacking sequence [45/−45/0/...], this crack orientation indicates fiber cracking from the first to the third ply.

Notably, the damage is not limited to the impact location but additional delamination occurred under the stiffening elements, as the D-Scan images show. This damage is either a debonding of the stiffeners from the skin or a delamination inside the stiffener foot. This damage is unwanted as the investigation focuses on the propagation of the primary impact damage in the skin at the impact spot. Particularly, a damage propagation into the stiffener would mark a significant difference from the DT behavior in a monolithic skin laminate. To determine the location of the secondary damage and its influence on the damage evolution, one panel was analyzed through a computer tomography (CT) scan after the ultimate failure in the compression test.

The comparison of the impact damage of the panels with the damage observed during the coupon study [16] reveals already some differences. These differences are quantified by the arrows in the last column of Table 1. Particularly, the projected delamination area of the panels is much larger than the corresponding coupon result, even though the impact energy was determined to cause a similar damage. To explain this difference, we compare the characteristic values of the impacts on both scales: the energy absorption is nearly equal, the maximum contact force is slightly lower on the panel level. Both observations suggest, that a too high impact energy is not the reason for the larger damage. The reason for the difference is likely a qualitatively different damage evolution during the impact: the limited size of the CAI coupon caused a boundary effect limiting the damage propagation. The observed difference has to be considered for the following compression tests and for the comparison of the DT behavior on both scales.

4.2. Quasi-static compression result

The first panel with the number P66 was subjected to a quasi-static collapse test which provides the reference residual strength. The measured ultimate load of this test is defined as a load level of 100 % for the cyclic testing of the other two specimens. Further, the observed failure mode permits a first assessment of the panel's DT.

The recorded force displacement response is shown in Fig. 8 and reveals a linear behavior until ultimate failure. (The load decrease at 150 kN in the curve of specimen P66 was caused by a time hold at the corresponding displacement level, during this time hold the specimen apparently showed a relaxation effect.) The collapse occurred

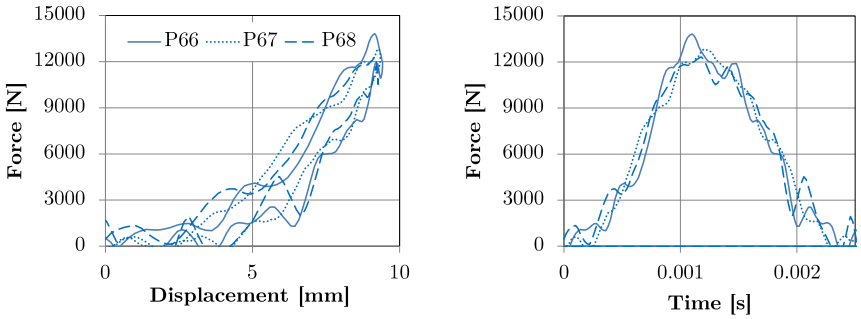

Fig. 7. Set of history curves of the 42 J impacts on the center of the substructure panels.

Table 1
The characteristic values and the respective standard deviation of the panel impact tests with 42 J.

Parameter	Unit	P66	P67	P68	Comparison with avg. coupon result
Impact energy	[J]	42.1	41.7	42.9	↑
Impactor mass	[kg]	0.835	0.835	0.835	↓↓↓
Max. contact force	[kN]	13.8	12.8	12.3	↓
Contact duration	[ms]	2.4	2.3	2.3	↓↓
Energy absorption	[J]	17.6	16.8	17.4	→
Proj. delamination	[mm²]	2850	3030	3530	↑↑↑
Visible fiber crack	[mm]	23	33	34	↑

Table 2
Load levels with the respective force parameters and the maximum nominal strain for the panel CCAI tests.

Load level	F_{max}	F_{min}	F_{amp}	ϵ_{max} (nominal)
100 %	315 kN	31.5 kN	141.8 kN	4500 με
80 %	252 kN	25.2 kN	113.4 kN	3600 με

at an axial load level of 315 kN which corresponds to a measured strain level of 4500 με on the panel's stiffened side, determined through digital image correlation (DIC). The load parameters derived from the quasi-static test of the specimen P66 are provided in the Table 2. In comparison with the CAI coupon tests, the strain level is lower in case of the panels. The significantly larger delamination area of the panels in comparison to the coupons is a likely explanation for this decrease.

As the ultrasonic scan after the collapse shows in Fig. A.16, the impact damage propagated in lateral direction, perpendicularly to the loading direction. This damage propagation pattern is similar to that on the CAI coupons. In addition, the horizontal fiber crack in the 0° plies propagates as a kink band through the entire panel width. However, the results of this test do not provide any evidence to determine which of these failure modes caused the collapse. In addition, the stiffeners begin to separate from the skin laminate (or delaminated within the stiffener foot). Apart from that, the stiffeners were found undamaged even after ultimate failure. As a consequence of the intact stiffeners, the load dropped only to 198 kN after the collapse, which means that failed structure still sustains around 60 % of the ultimate load. With regard to the load transfer from the skin to the stiffeners as a second load path, this is a positive DT characteristic.

Apart from the quasi-static collapse test of P66, also the tests of the panels P67 and P68 each began with a quasi-static step before the cyclic load intervals. In this first cycle, the specimens were subjected to the peak force of the cyclic load F_{max}. As the cyclic loading was conducted on a load level of 80 %, F_{max} corresponds to 252 kN. The respective force displacement responses of each specimen's first cycle ($n = 1$) are also included in Fig. 8. These curves reveal that the initial stiffness (below 150 kN) of all panels is nearly equal. The relaxation during the hold period of P66 does not permit a further comparison of the curves. However, P68 exhibited a stiffness decrease through two minor load drops. Thus the secant stiffness at the load maximum of P68 was around 5 % lower than that of P67.

Further quasi-static load cycles were conducted repeatedly throughout the cyclic testing procedure of P67 and P68. During these quasi-static load cycles, DIC measurements were conducted, the specimen stiffness was determined, and high-sampled force displacement curves were recorded. The diagram in Fig. 8 also includes each panel's last quasi-static test before the collapse under cyclic load. In the discussion section referring to the cyclic test, the decrease of the stiffness during the cyclic loading is further analyzed.

4.3. Cyclic compression after impact results

A quasi-static test provides information about the residual strength and the failure mechanism of an impact-damaged composite panel. The cyclic tests complement this data through revealing the DT failure at a smaller load level. In fact, a cyclic test can enable a better understanding of the failure mechanisms as it permits us a more accurate observation of the damage evolution throughout the test. Nonetheless, the damage mechanism itself can differ between cyclic and quasi-static loading.

Quantitative information about the DT failure of P67 and P68 is provided through the endurance, the evolution of the stiffness as shown in Fig. 9, and the detected growth of the delamination in Fig. 12. The stiffness of the panel is calculated from the measurement data of the testing machine and the delamination area results from an evaluation of the ultrasonic scans. For a qualitative interpretation of the damage evolution we take into account the ultrasonic scans shown in Fig. A.16, the visible damage propagation on the panel surface shown in Fig. A.17, and the DIC measurements (Fig. A.18) from the quasi-static load cycles. Furthermore, the evaluation of the ultrasonic scans allows us to obtain the damage area depending on the load cycles as shown in Fig. 12. In addition, the stiffness of the panel is calculated from the measurement data of the testing machine (cf. 9). The ensemble of these results permits us to interpret the mechanisms of the damage evolution which results in the ultimate DT failure under cyclic load.

P67 and P68 failed after 2672 and 2426 cycles. Remarkably, both tests began with a long period without detectable damage growth. Even though during the few first cycles of both panels some cracking sounds were heard, there was no detectable difference in the damage. Also the stiffness of the panels hardly decreases during this no-growth interval. The damage propagation began suddenly and resulted in the collapse of the corresponding panel within few cycles. This behavior meets the expectations and also corresponds to the experimental outcomes published by other researchers [22–25,37].

During the test of P67, the ultrasonic scan revealed no change of the damage size or shape after an interval of 1840. A significant cracking noise could be heard after 2660 cycles. In consequence, the loading sequence was interrupted for an ultrasonic scan which revealed an increase of the delamination in the upper interfaces of the skin

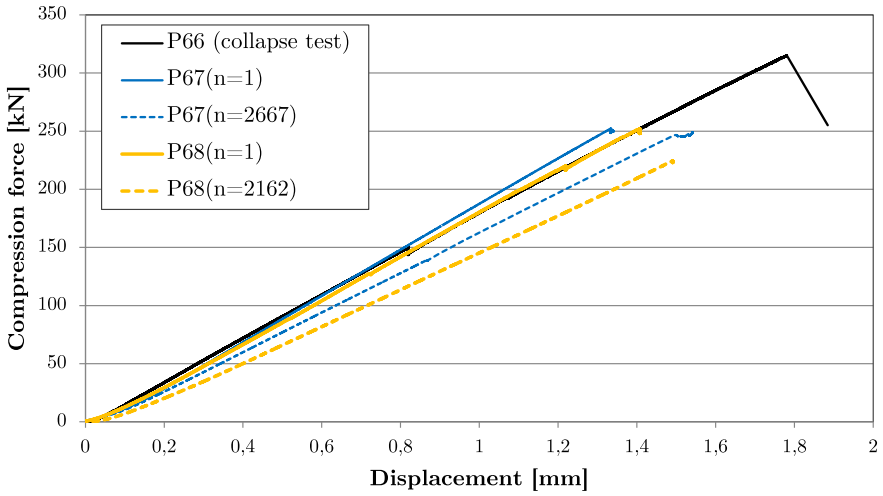

Fig. 8. Force–displacement curves of the quasi-static test of all three stiffened panels. P66 was tested until ultimate failure occurred.

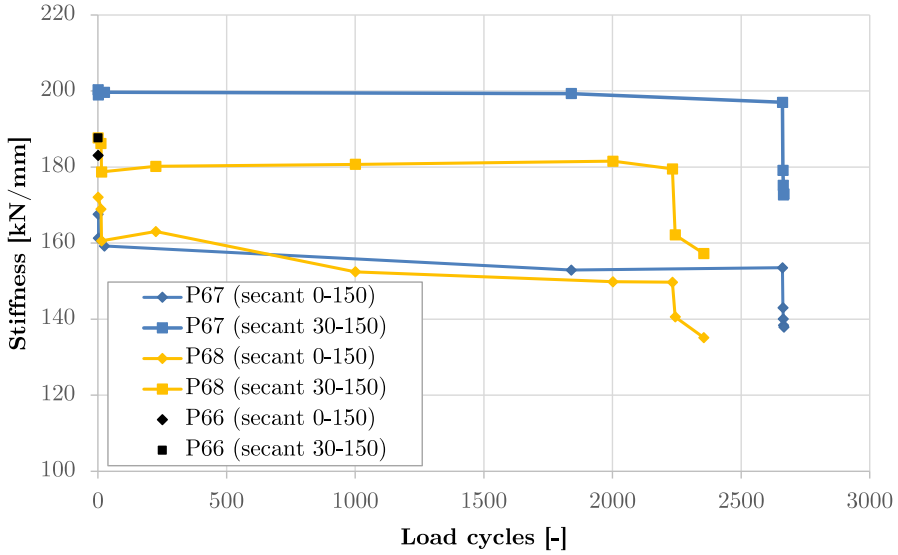

Fig. 9. Force–displacement curves of the quasi-static test of all three stiffened panels. P66 was tested until ultimate failure occurred.

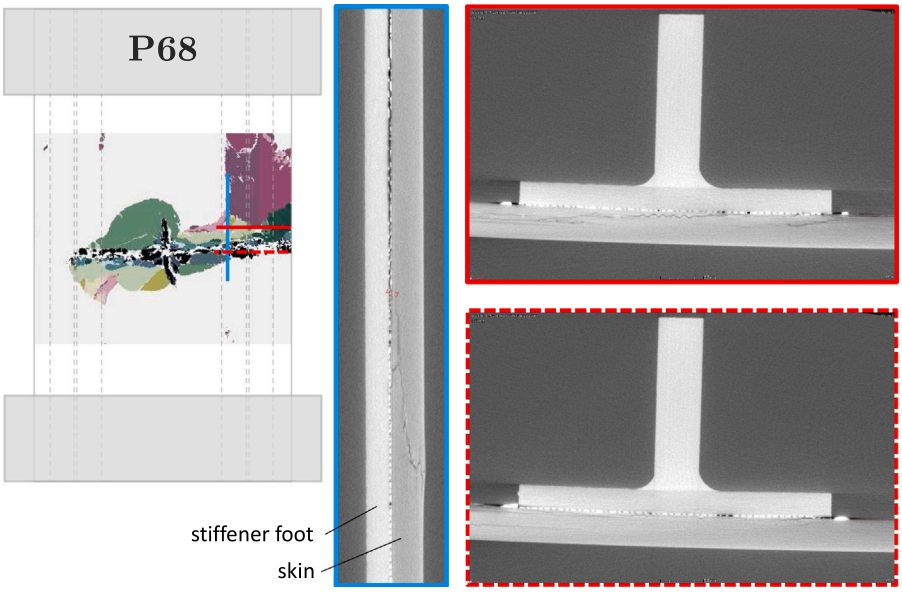

Fig. 10. CT scan of P68 after ultimate failure. The cross section images show the skin damage, the undamaged stiffener and its debonding from the skin.

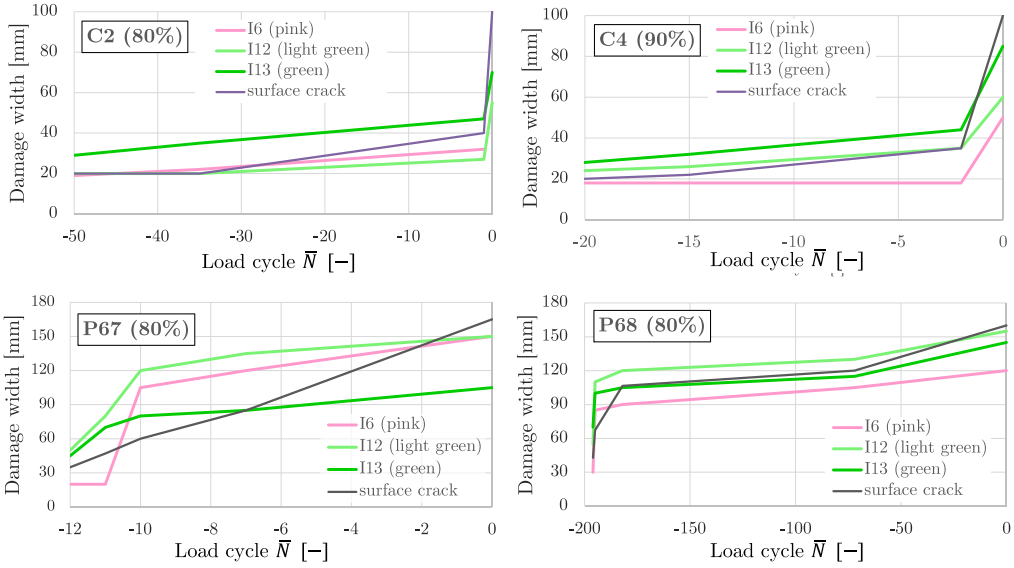

Fig. 11. Damage growth history in individual delamination interfaces and the surface crack on two exemplary coupon specimens (C2 and C4 in Fig. A.15) and the panels P67 and P68. $\overline{N}$ refers to the number of cycles until final failure. (For interpretation of the references to color in this figure legend, the reader is referred to the web version of this article.)

laminate (close to the impact side). This lateral delamination propagation was accompanied by a growth of the visible fiber crack in the same direction. After each following load cycle a significant damage growth damage was observed. During this short interval of damage growth, the delamination and the fiber cracking propagated to both direction. The collapse occurred only 12 cycles after the first detection of damage growth. These twelve cycles revealed also a significant reduction of the specimen stiffness which adds up to 12 % directly before the ultimate failure. The mode of the propagation – a growth of the delamination and the fiber fracture in lateral direction – is similar to the quasi-static test. Prior to these twelve final cycles, only the DIC measurement revealed an ongoing change of the impact damage: after 1860 cycles, the maximum out-of-plane deformation measured at F_{max} nearly doubled to 0.57 mm in comparison to the first load cycle with 0.32 mm. Another doubling to 1.33 mm occurred until the beginning of the damage propagation at cycle number 2660.

The test of P68 was conducted with an adapted control mode to achieve an improved understanding of the damage propagation phase. The load-controlled test forwards the damage propagation when the specimen stiffness decreases. To achieve a slower damage progression, the test mode of P68 was switched to displacement control after the first detectable damage propagation began. During the displacement-controlled phase, the test of P68 began with similar observations like the P67 test. After 2001 load cycles, only a minimal growth of the uppermost delamination was visible in the ultrasonic scan. At that time, the fiber crack grew by 2 mm. After 2230 cycles, a load cracking noise gave evidence of significant damage propagation. However, the cyclic loading could only be stopped with a delay of one cycle which further propagated the damage. Thus, the displacement control was applied after 2331 load cycles. The displacement parameters from the cycle 2231 were used for subsequent cycles. Hence, any further damage propagation decreases the applied load. This approach corresponds to the existence of a very stiff alternative load path in a real structure to which the load of the damaged section gets transferred. As opposed to the load controlled test, representing a structure with no alternative load paths, displacement control is the least conservative possibility. It was chosen in order to discover whether a stabilization of the damage propagation could possibly be achieved. Indeed, the switch to displacement control significantly slowed down the damage propagation. After the 2331 cycles under load control, P68 endured another 193 cycles under displacement control. This interval marks the period of damage propagation. In case of the load-controlled test of P67 this period lasted only 12 cycles. This is an increase by a factor of approx. fifteen. Despite this increase, the behavior under displacement control can still not seen as a significant stabilization. In relation to the 2000 cycles before the initiation of the propagation, the phase of damage propagation is around 10 % of the total panel life span until ultimate failure. During these 193 cycles, the maximum force $F_{max}(N)$ dropped to a value of 222 kN in the cycle number 2671. This corresponds to a stiffness decrease of 12 %. Similar to the observation during the P67 test, the DIC measurement on the back side of the panel revealed an increase of the out-of-plane deformation from 0.44 mm to 0.99 mm within the first 2001 cycles. The bigger part of this increase happened in an early stage of the test, as a doubling to 0.88 mm was already reached after 225 load cycles. This phenomenon was the earliest detectable sign of a damage-related change in the specimen.

Qualitatively, the delamination and the fiber kink band propagate laterally to both sides. However, the phenomenon of the damage propagation can be analyzed in deeper detail than during the quasi-static test. Particularly, the D-Scan images in Fig. A.16 permit us to recognize the delamination in the individual interfaces of the laminate. Notably, the first delamination growth does not initiate from the largest delaminations in the central interfaces of the laminate. Instead, the propagation begins in the topmost interfaces, closes to the impact side (P67 at the cycle 2660, P68 at the cycle 2001). Most of the observed fiber cracking is located in the topmost plies next to these interfaces where the first damage growth could be observed. This observation suggests a correlation of the fiber kinking and the delamination propagation. A comparison of the delamination length and the visible fiber crack length reveals the delamination tip located ahead of the fiber crack. During the further damage evolution, also the delaminations in the central interfaces (green colors in the D-scan), and in the bottom-near interfaces (pink colors in the D-Scan) begin to grow. These observations suggest a crucial influence of the fiber failure to the damage evolution – a perception which has already been proposed by other researchers: Based on CAI experiments, Nettles and Scharber [48] conclude ply failure due to stress concentration to be the predominant failure mode in a CAI load case.

An interaction of the centric impact damage and the stiffener debonding was not observed before the ultimate failure. In relation to the DT, this is a positive perception. Furthermore, the intact stiffeners after the collapse evidence a fail-safe behavior. The second load path

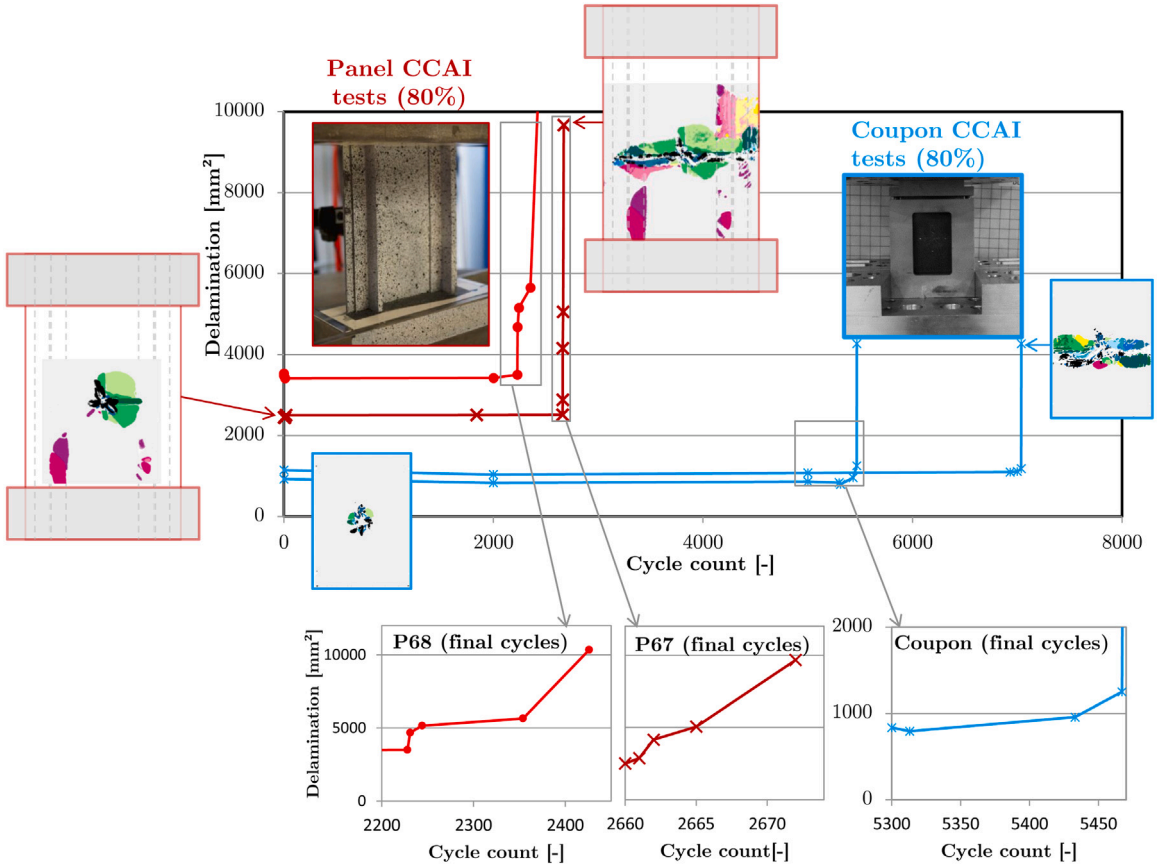

Fig. 12. Delamination growth in the stiffened panel in comparison with the analog coupon results.

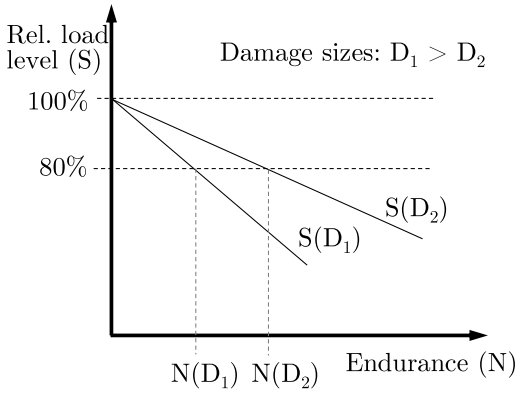

Fig. 13. Hypothesis for the influence of the damage size to the dimensionless S-N-curve (the interval until damage growth onset is considered as the endurance (N).

through the stiffeners is hardly damaged during the failure of the skin. To affirm the collapsed panel P68 was subjected to a CT scan. Three cross section images from this scan are shown in Fig. 10. These images reveal that delamination under the stiffener is indeed a debonding at the interface. Further, a delamination was found in the interfaces on the backside of the skin. The stiffener was found undamaged in the entire scanned region.

4.4. Comparison between the panel and the coupon level

The results of the presented panel tests have to be interpreted in the context of the results of the CCAI coupon tests published in a previous paper [16]. The damage evolution, quantified through the projected delamination area, is depicted in Fig. 12 for both the panel and the coupon experiments as a direct comparison. Several qualitative similarities were observed on both scales:

- After a considerable interval without detectable damage growth, the damage suddenly begins to propagate, initiating the collapse within few load cycles. The amount of load cycles concerned by the damage propagation is less than 1 % of the respective endurance.
- The delamination and the fiber kink band propagate perpendicularly to the loading direction to both sides of the specimen.
- The specimen stiffness remains constant throughout the no-growth interval and begins to decrease measurably with the damage propagation.

4.4.1. Damage growth investigation

To compare the damage growth behavior on the coupon level and on the panel level, the growth history of the delamination is evaluated. For this investigation we zoom into the damage propagation period observed in the experiments. Fig. 11 depicts the damage progression of delamination at three individual interfaces. Counting from the bottom side of the laminate, we considered the 6th, the 12th and the 13th interface of the layup which are depicted in pink, light green, and green, respectively in Fig. A.15. The colors in the plot correspond to the color in the ultrasonic D-Scan images and to the indicated interfaces in the layup from the stiffener side to the outer side (impacted side): $[-45, 45, 0, 90, -45, 45||0, 90, -45, 45, 0, 90||-45||45, 0, 90, 90, 0, 45, -45, 90, 0, 45, -45, 90, 0, 45, -45, 90, 0, 45, -45]$
As the damage propagates mainly in the lateral direction, the damage width is used as a metric for this analysis. $\overline{N}$ references the load cycle before ultimate failure ($\overline{N} = 0$). This detailed damage growth

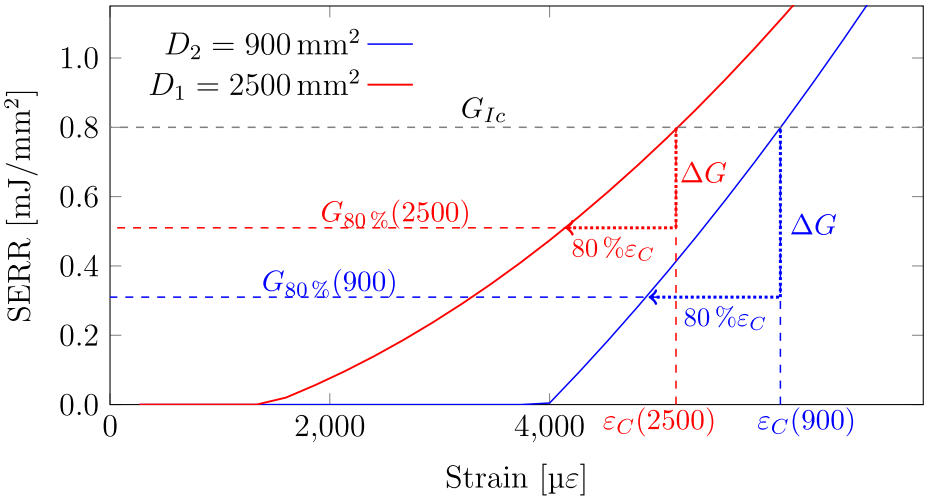

Fig. 14. Calculated ERR at the delamination front for the damage sizes observed on the coupon and on the panel.

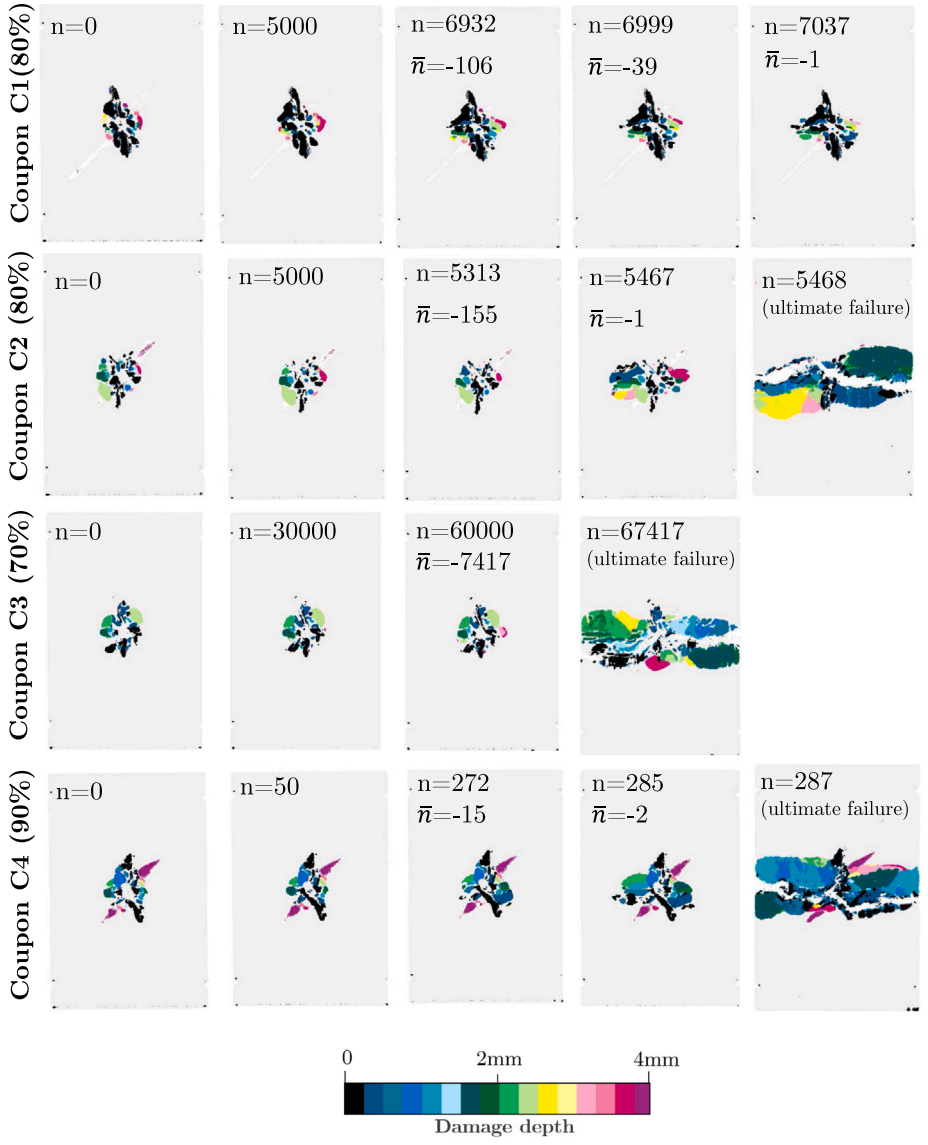

Fig. A.15. Observation of the delamination growth in the ultrasonic D-scan of four selected CCAI experiments with 100×150 mm^2 coupon specimens (published in [16]).

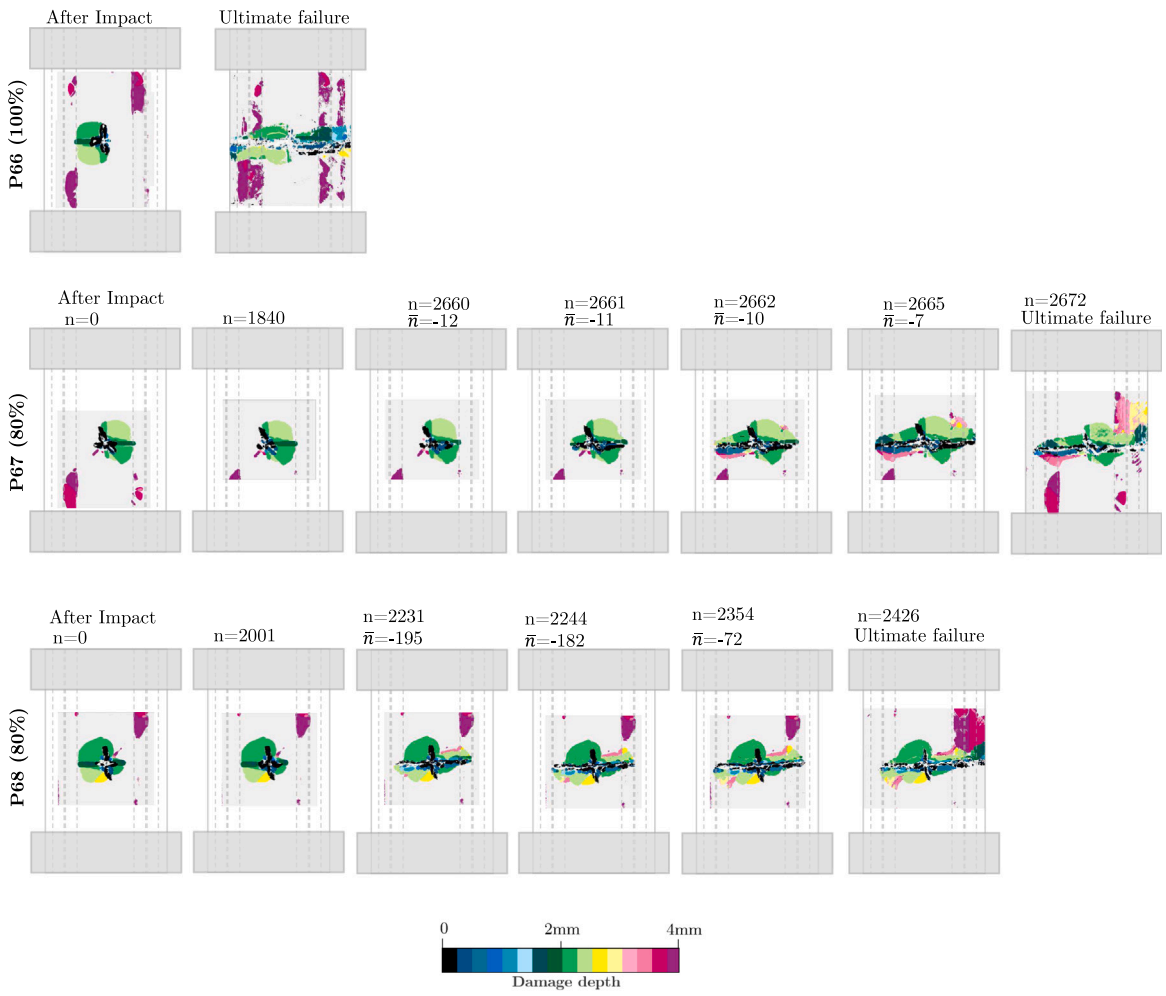

Fig. A.16. Ultrasonic D-scans of the three each panel throughout its test. Each scan is depicted in a sketch of the specimen to show the damage evolution in relation to the panel geometry. (For interpretation of the references to color in this figure legend, the reader is referred to the web version of this article.)

evaluation is conducted for both cyclic panel tests (P67 and P68) and for two exemplary coupon tests where ultrasonic inspections were conducted in close intervals (C2 and C4 in Fig. A.15).

With regard to the entire cyclic test, the damage growth initiates suddenly on both scales and progressively leads to the final failure. However, a detailed investigation reveals a considerable difference in the damage evolution of the coupons and the panels. After the initiation of the damage growth on the coupon level, the damage grows indeed progressively and leads to sudden ultimate failure in an exponential-like damage propagation curve. This behavior can be captured through a damage growth law like the Paris–Erdogan law [49], exponentially correlating the damage growth rate $\frac{da}{dN}$ with the strain energy release rate (SERR) ΔG at the delamination crack tip. However, due to the very short interval of actual damage propagation and the sparse data points, a quantitative interpolation of the coefficients of this law does not make sense on the basis of these experiments. Slight uncertainties in the measured data would cause severe uncertainties in the derived parameters. Instead, cyclic fracture-mechanical characterization tests would have to be conducted, for example as proposed by Kruger [50].

With regard to the damage propagation during the panel test, a short period of damage stabilization is visible in the respective curves in Fig. 11. After an initial sudden damage growth as we have seen it during the coupon experiments, a flattening occurs and the further damage propagation slows down. In case of P68 this phenomenon could be explained through the displacement-controlled test procedure. However, also the test of P67 revealed such a behavior, thus, there has to be an additional reason for the declining damage growth. Notably, the curves flatten at a damage width of 120 mm which corresponds to the distance of the stiffeners. Thus, the results suggest that the stiffeners are the cause of the slowed down delamination propagation. This phenomenon is comparable to the slow down of the crack growth in an isotropic structure. According to the structural analysis handbook HSB [3], this slow down can be included in the damage propagation law through a modification of the SERR driving the damage growth. Hence, describing the damage propagation through the above-mentioned Paris–Erdogan law is still valid. Nonetheless, the SERR at the crack tip has to be determined under the consideration of the stiffeners in order to conduct a plausible prediction.

For the surface cracks on the coupons and panels no distinct damage growth behavior can be stated since the curves in Fig. 11 exhibit both exponential-like and linear-like behavior. Nevertheless, different failure types concerning the surface crack could be observed. The panels obtain surface cracks on the impact side whereas the CCAI coupons in a previous paper [16] exhibit fiber breakage on the back side. Surprisingly, the failure type of the panels resembles the quasi-static failure type of the CCAI coupons. A possible reason for this failure type could be the force transmission of the stringers on the backside of the panels preventing fiber breakage on the outer backside of the panels.

4.4.2. *No-growth interval depending on the damage size*

Remarkably, the damage growth begins suddenly on both scales. To account for such a damage evolution behavior in a DT design,

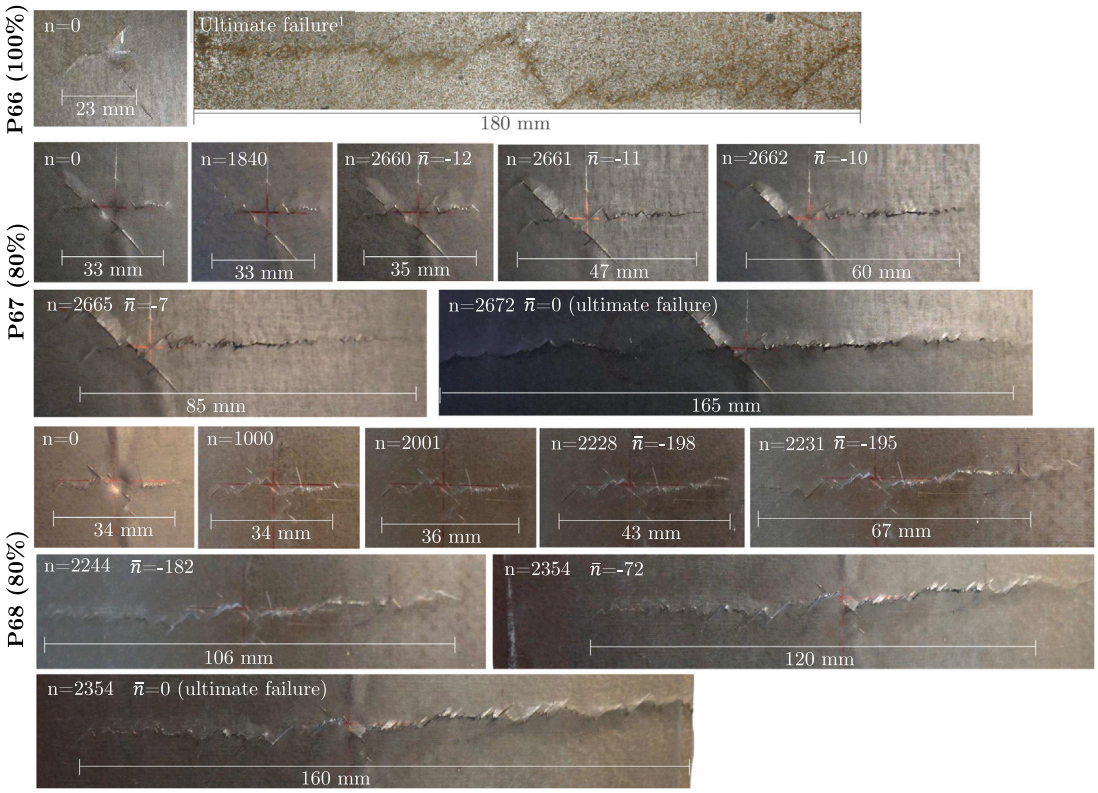

Fig. A.17. Evolution of the fiber cracking on the impact side of each panel throughout its test.[1]

a no-growth approach has to be employed. The interval until the initiation of the damage propagation has to be considered as the design-relevant endurance for the corresponding strain level. Nonetheless, this endurance value was found to be considerably lower during the panel tests in comparison with the coupon tests — despite equal relative load levels (80 % of the quasi-static strength). The nominal strain level of the panel tests is even smaller than the nominal strain level of the coupon tests. This divergence has to be explained. While the panel skin laminate equals that of the coupon specimens, a crucial difference of the initial condition between the two scales emerges with the impact damage. The delamination observed in the panels is significantly larger than the delamination observed in the coupon tests. In detail, sizable delaminations in interfaces in the center of the laminate increase the projected delamination area.

We investigate the difference of the damage size as a possible cause for the differing endurance. Particularly, the influence of the damage size D on the endurance N has to be understood for a given relative load level S. On the basis of the S-N-curve with a relative load axis in Fig. 13, we hypothesize a negative correlation of D and N for a constant load level S. The condition in Eq. (2) expresses this hypothesis.

$$N\left(S_I, D_1\right) < N\left(S_I, D_2\right) \qquad for \qquad D_1 > D_2 \quad and \quad S_I < 100\% \tag{2}$$

The experimental results represent only two data points for each curve in the S-N diagram – $N(80\,\%, D_1)$ and $N(80\,\%, D_2)$. The experimental result reveals a correlation of $N(80\,\%, D_1) < N(80\,\%, D_2)$ which implies an increasing gradient $-\frac{\partial S}{\partial N}$ for an increasing damage size D. To proof this hypothesis, the phenomenology driving the damage propagation under compression load shall be considered. According to Rhead et al. [12], the buckling of sublaminates results in a mode I opening of the delamination cracks. The SERR at the delamination tip correlates non-linearly with the strain level. Through the analysis method of Bogenfeld et al. [51], this correlation can be calculated for the damage sizes $D_1 = 2500$ mm^2 and $D_2 = 900$ mm^2 (cf. Fig. 14). The SERR becomes greater zero as soon as a sublaminate begins to buckle. Afterward, the SERR increases non-linearly. The quasi-static failure corresponding to a load level of $S = 100\,\%$ is marked through the SERR exceeding the critical value G_{Ic}. The respective failure strain level is ε_c of each curve in Fig. 14. The reduction of the load in the cyclic test proportionally reduces the strain level on the basis of ε_c.

The difference of the SERR ΔG for a reduced strain level can be linearized to the product of the strain difference $\Delta\varepsilon$ and the gradient (Eq. (3)).

$$\Delta G \approx \Delta\varepsilon \frac{\partial G}{\partial \varepsilon} \tag{3}$$

Two factors result in the value $G_{80\,\%}(900)$ being lower than $G_{80\,\%}(2500)$:

- The first factor $\Delta\varepsilon$ is proportional to ε_c, hence, it decreases for increasing damage size (Eq. (4)).

$$\Delta\varepsilon(D_1) > \Delta\varepsilon(D_2) \tag{4}$$

- The SERR depends on the available strain energy in the laminate when the sublaminate begins to buckle [51] which correlates with ε^2. Hence, a smaller damage which buckles later results in a larger gradient as given in

$$\left.\frac{\partial G}{\partial \varepsilon}\right|_{D_1} < \left.\frac{\partial G}{\partial \varepsilon}\right|_{D_2} \quad for \qquad D_1 > D_2 \tag{5}$$

The SERR and the endurance can be considered monotonically correlated [50]. According to this correlation, the analysis approves the hypothesis that the damage is a likely cause of the endurance difference found between the experiments on both scales.

[1] The surface of the panel P66 was painted with speckle pattern for the DIC measurement from the impact side. The paint worsened the visibility of the fiber crack on the photo.

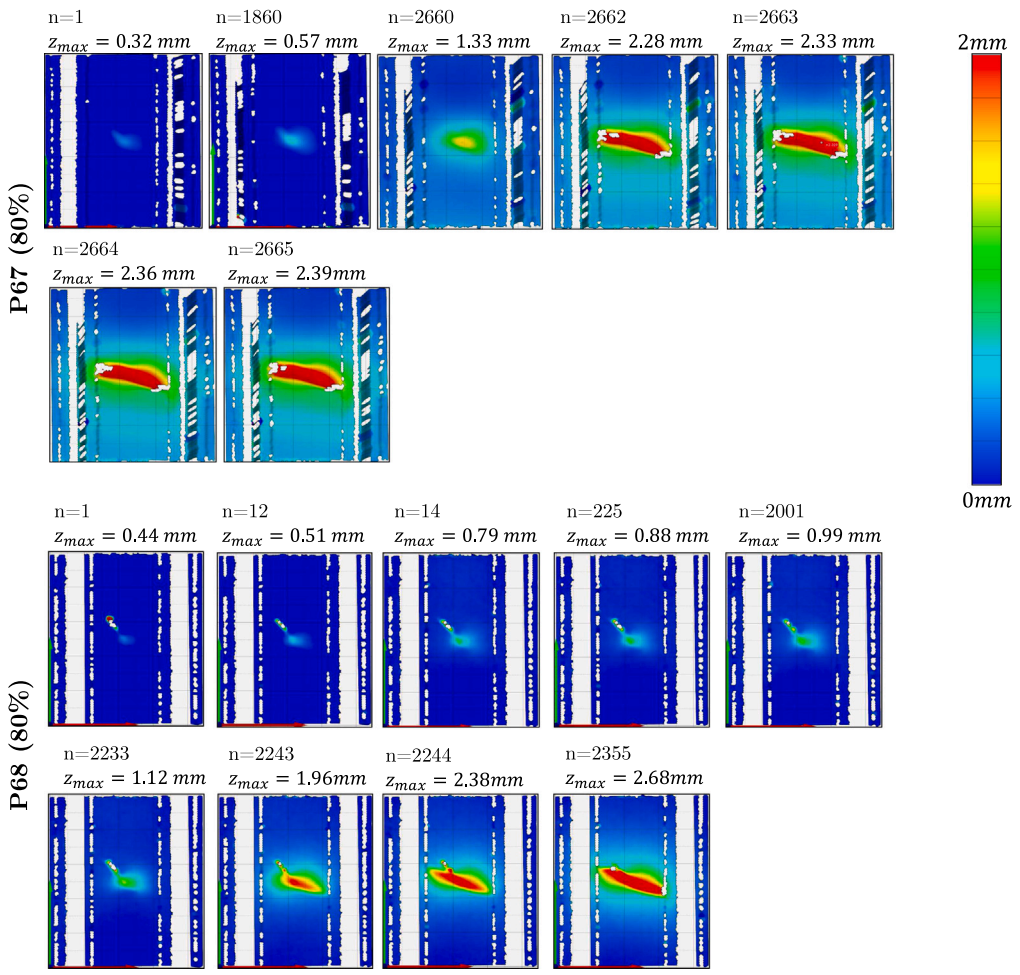

Fig. A.18. Out-of-plane displacement from the DIC measurements of the specimens P67 and P68 at the peak load (252 kN) of the quasi-static load cycles.

5. Conclusion and outlook

This experimental studied revealed the impact damage evolution behavior of stiffened panels under cyclic compression load. In total, three panel specimens were tested, one under quasi-static and two under cyclic loading conditions. The damage evolution was monitored through ultrasonic inspection, digital image correlation, and measurements of the stiffness. The study was carried out to supplement a previously conducted coupon test campaign with a similar laminate as the panel skin. The outcome of the panel experiments revealed a damage evolution qualitatively similar to the behavior on the coupon level. However, quantitative differences were observed during this study.

- The tests revealed a long no-growth period comprising more than 90 % of the specimen's fatigue life.
- During the no-growth interval, the only measurable change at the specimen is an increasing local out-of-plane deformation at the impact spot detected through the DIC.
- A sudden initiation of lateral propagation marks the ultimate failure of the structure under cyclic loading. The fiber crack on the impact side and the delamination propagate simultaneously.
- While the damage growth is purely progressive until final failure on the coupon level, the panel tests exhibit a declining propagation when the damage width approaches the stiffener distance.
- The damage propagation is limited to the panel skin. Even after the final failure, the stiffeners are still undamaged.

The quantitative comparison of the coupon and panel level shows that the endurance on a similar relative load level is lower on the panel level. However, an explanation through the different damage sizes in both test series could be found through an analytical analysis.

With regard to a damage-tolerant design, the results suggest the exploitation of the no-growth interval as the most suitable approach. The calculation of the no-growth endurance can be conducted on the coupon level. However, the differences of the design-relevant damage size on the structure have to be considered to achieve a conservative prediction of the no-growth interval. There is no evidence suggesting the possibility of a slow growth design as even the least conservative case, a closed-loop displacement control, did not stabilize the damage propagation. However, the tests also showed a favorable DT characteristic of the specimens. The damage growth is limited to the panel skin. The stiffeners remaining intact represent a second load path which is not affected by the impact damage propagation.

Declaration of competing interest

The authors declare that they have no known competing financial interests or personal relationships that could have appeared to influence the work reported in this paper.

Data availability statement

The raw data required to reproduce these findings cannot be shared at this time due to legal reasons.

Acknowledgments

All research was accomplished within the DLR projects KonTeKst and oLAF. The authors acknowledge the DLR for funding these projects.

Appendix. Result figures from the experiments

see Figs. A.15–A.18.

References

[1] Federal Aviation Administration, AC 25.571-1D Damage Tolerance and Fatigue Evaluation of Structure, 2011, http://dx.doi.org/10.1177/004728757301200242.
[2] S. Dubinskii, Y. Feygenbaum, V. Senik, E. Metelkin, A study of accidental impact scenarios for composite wing damage tolerance evaluation, Aeronaut. J. 123 (1268) (2019) 1724–1739, http://dx.doi.org/10.1017/aer.2018.152.
[3] IASB, Handbuch Struktur Berechnung, no. 2016, Struktur-Berechnungsunterlagen, Industrie-Ausschuss, 1976, pp. 1–20.
[4] A.A. Baker, R. Jones, R.J. Callinan, Damage tolerance of graphite/epoxy composites, Compos. Struct. 4 (1) (1985) 15–44, http://dx.doi.org/10.1016/0263-8223(85)90018-2.
[5] G. Newaz, R.L. Sierakowski, Damage Tolerance in Advanced Composites, Taylor & Francis, 1995, URL https://books.google.de/books?id=_hr1Ys1toA4C.
[6] Federal Aviation Administration, Advisory Circular: 20-107B - Composite Aircraft Structure, 2009.
[7] EASA, AMC 20-29 Composite Aircraft Structure - Annex II to ED Decision 2010/003/R of 19/07/2010, 2010, pp. 1–36.
[8] P. Goudou, Decision No 2010/003/R of the Executive Director of the European Aviation Safety Agency, Tech. rep., Cologne, 2010, URL https://www.easa.europa.eu/sites/default/files/dfu/EDDecision2010_003_R.pdf.
[9] M. Mitrovic, H.T. Hahn, G.P. Carman, P. Shyprykevich, Effect of loading parameters on the fatigue behaviour of impact damaged composite laminates, Compos. Sci. Technol. 59 (1999) 2059–2078, http://dx.doi.org/10.1016/S0266-3538(99)00061-5.
[10] G. Davies, P. Irving, Impact, Post-Impact Strength and Post-Impact Fatigue Behaviour of Polymer Composites, Elsevier Ltd, 2014, pp. 231–259, http://dx.doi.org/10.1016/B978-0-85709-523-7.00009-8.
[11] G. Clark, T.J. Van Blaricum, Load spectrum modification effects on fatigue of impact-damaged carbon fibre composite coupons, Composites 18 (3) (1987) 243–251, http://dx.doi.org/10.1016/0010-4361(87)90414-9.
[12] A.T. Rhead, R. Butler, G.W. Hunt, Compressive strength of composite laminates with delamination- induced interaction of panel and sublaminate buckling modes, Compos. Struct. 171 (2017) 326–334, http://dx.doi.org/10.1016/j.compstruct.2017.03.011.
[13] C.P. Dienel, H. Meyer, M. Werwer, C. Willberg, Estimation of airframe weight reduction by integration of piezoelectric and guided wave–based structural health monitoring, Struct. Health Monit. (2018) http://dx.doi.org/10.1177/1475921718813279.
[14] T.A. Sebaey, E.V. González, C.S. Lopes, N. Blanco, J. Costa, Damage resistance and damage tolerance of dispersed CFRP laminates: Design and optimization, Compos. Struct. 95 (2013) 569–576, http://dx.doi.org/10.1016/j.compstruct.2012.07.005.
[15] N. Dubary, C. Bouvet, S. Rivallant, L. Ratsifandrihana, Damage tolerance of an impacted composite laminate, Compos. Struct. 206 (July) (2018) 261–271, http://dx.doi.org/10.1016/j.compstruct.2018.08.045.
[16] R. Bogenfeld, C. Gorsky, An experimental study of the cyclic compression after impact behavior of CFRP composites, J. Compos. Sci. 5 (296) (2021) http://dx.doi.org/10.3390/jcs5110296.
[17] J. Baaran, Study on Visual Inspection of Composite Structures EASA-Research Project/2007/3 - Final Report, Tech. rep., EASA, 2009, URL https://www.easa.europa.eu/sites/default/files/dfu/EASA_REP_RESEA_2007_3.pdf.
[18] I. Papa, M.R. Ricciardi, V. Antonucci, A. Langella, J. Tirillò, F. Sarasini, V. Pagliarulo, P. Ferraro, V. Lopresto, Comparison between different non-destructive techniques methods to detect and characterize impact damage on composite laminates, J. Compos. Mater. 54 (5) (2020) 617–631, http://dx.doi.org/10.1177/0021998319864411.
[19] M. Moix-Bonet, B. Eckstein, P. Wierach, Probability - based damage assessment on a composite door surrounding structure, in: 8th European Workshop on Structural Health Monitoring (EWSHM), no. July, Bilbao, Spain, 2016, pp. 5–8, URL https://elib.dlr.de/117046/.
[20] S. Sikdar, S. Banerjee, Structural Health Monitoring of Advanced Composites using Guided Waves, no. September, first ed., Lambert Academic Publishing, Beau Bassin, ISBN: 978-620-2-02697-0, 2017.
[21] A. Nettles, A. Hodge, J. Jackson, An examination of the compressive cyclic loading aspects of damage tolerance for polymer matrix launch vehicle hardware, J. Compos. Mater. 45 (4) (2011) 437–458, http://dx.doi.org/10.1177/0021998310376117.
[22] G. Davies, P. Irving, 9 - Impact, post-impact strength and post-impact fatigue behaviour of polymer composites, in: Polymer Composites in the Aerospace Industry, Elsevier Ltd, 2015, pp. 231–259, http://dx.doi.org/10.1016/B978-0-85709-523-7.00009-8.
[23] L.G. Melin, J. Schön, Buckling behaviour and delamination growth in impacted composite specimens under fatigue load: An experimental study, Compos. Sci. Technol. 61 (13) (2001) 1841–1852, http://dx.doi.org/10.1016/S0266-3538(01)00085-9.
[24] D.D. Symons, G. Davis, Fatigue testing of impact-damaged T300/914 carbon-fibre-reinforced plastic, Compos. Sci. Technol. 60 (2000) 379–389, http://dx.doi.org/10.1016/S0266-3538(99)00138-4.
[25] N. Uda, K. Ono, K. Kunoo, Compression fatigue failure of CFRP laminates with impact damage, Compos. Sci. Technol. 69 (14) (2009) 2308–2314, http://dx.doi.org/10.1016/j.compscitech.2008.11.031.
[26] D.S. Saunders, T.J. Van Blaricum, Effect of load duration on the fatigue behaviour of graphite/epoxy laminates containing delaminations, Composites 19 (3) (1988) 217–228, http://dx.doi.org/10.1016/0010-4361(88)90240-6.
[27] A.S. Chen, D.P. Almond, B. Harris, In situ monitoring in real time of fatigue-induced damage growth in composite materials by acoustography, Compos. Sci. Technol. 61 (16) (2001) 2437–2443, http://dx.doi.org/10.1016/S0266-3538(01)00165-8.
[28] L. Molent, A. Haddad, A critical review of available composite damage growth test data under fatigue loading and implications for aircraft sustainment, Compos. Struct. 232 (July 2019) (2020) 111568, http://dx.doi.org/10.1016/j.compstruct.2019.111568.
[29] Airbus Industries, AITM 1-0010 Determination of Compression Strength After Impact, Airbus S.A.S Engineering Directorate, Blagnac, 2005, pp. 1–15.
[30] ASTM and ASTM International, ASTM D7136 - Standard Test Method for Measuring the Damage Resistance of a Fiber-Reinforced Polymer Matrix Composite to a Drop-Weight Impact Event, 2005, http://dx.doi.org/10.1520/D7136.
[31] ASTM D7137 - Standard Test Method for Compressive Residual Strength Properties of Damaged Polymer Matrix Composite Plates, ASTM International, West Conshohocken, PA, 2007, http://dx.doi.org/10.1520/D7137_D7137M-17, URL http://www.astm.org/cgi-bin/resolver.cgi?D7137D7137M-17.
[32] Z.P. Bazant, Fracture in concrete and reinforced concrete, in: Mech of Geomater, Rocks, Concr, Soils (1968), 1985, pp. 259–303, http://dx.doi.org/10.1016/0148-9062(86)92639-2.
[33] Z.P. Bažant, J.J.H. Kim, I.M. Daniel, E. Becq-Giraudon, G. Zi, Size effect on compression strength of fiber composites failing by kink band propagation, Int. J. Fract. 95 (1–4) (1999) 103–141, http://dx.doi.org/10.1007/978-94-011-4659-3_7.
[34] A. Soto, E.V. González, P. Maimí, J.A. Mayugo, P.R. Pasquali, P.P. Camanho, A methodology to simulate low velocity impact and compression after impact in large composite sti ff ened panels, Compos. Struct. 204 (July) (2018) 223–238, http://dx.doi.org/10.1016/j.compstruct.2018.07.081.
[35] R. Tan, Z. Guan, W. Sun, Z. Liu, J. Xu, Experiment investigation on impact damage and influences on compression behaviors of single T-stiffened composite panels, Compos. Struct. 203 (July) (2018) 486–497, http://dx.doi.org/10.1016/j.compstruct.2018.07.038.
[36] R. Tan, J. Xu, Z. Guan, W. Sun, T. Ouyang, S. Wang, Thin-walled structures experimental study on effect of impact locations on damage formation and compression behavior of stiffened composite panels with L-shaped stiffener, Thin-Walled Struct. 150 (February) (2020) http://dx.doi.org/10.1016/j.tws.2020.106707.
[37] Y. Feng, Y. He, H. Zhang, X. Tan, T. An, J. Zheng, Effect of fatigue loading on impact damage and buckling/post-buckling behaviors of stiffened composite panels under axial compression, Compos. Struct. 164 (2017) 248–262, http://dx.doi.org/10.1016/j.compstruct.2016.12.069.
[38] Solvay, FM 300 Technical Data Sheet, 2018, URL https://www.solvay.com/en/product/fm-300.
[39] S. Mall, W.S. Johnson, Characterization of Mode I and Mixed-Mode Failure of Adhesive Bonds between Composite Adherends, Tech. Rep. NASA-TM-86355 19850012960, NASA, Hampton, Virginia, 1985.
[40] J.M. Whitney, A.C.D.-. on High Modulus Fibers, T. Composites, Composite Materials: Testing and Design (seventh Conference) : a Conference : Philadelphia, PA, 2-4 April 1984, ASTM STP 893, ASTM, 1986, URL https://books.google.de/books?id=eHU380PzDsQC.
[41] C. Balzani, W. Wagner, D. Wilckens, R. Degenhardt, S. Büsing, H.-G. Reimerdes, Adhesive Joints in Composite Laminates – A Combined Numerical / Experimental Estimate of Critical Energy Release Rates, Tech. rep., Karlsruher Institut für Technologie, 2011.
[42] R. Bogenfeld, J. Kreikemeier, T. Wille, Review and benchmark study on the analysis of low-velocity impact on composite laminates, Eng. Fail. Anal. 86 (April 2018) (2018) 72–99, http://dx.doi.org/10.1016/j.engfailanal.2017.12.019, URL http://linkinghub.elsevier.com/retrieve/pii/S1350630717309755.
[43] A. Gliszczynski, R. Bogenfeld, R. Degenhardt, T. Kubiak, Corner impact and compression after impact (CAI) of thin-walled composite profile – An experimental study, Compos. Struct. 248 (March) (2020) 112502, http://dx.doi.org/10.1016/j.compstruct.2020.112502.

[44] R. Bogenfeld, J. Kreikemeier, T. Wille, An analytical scaling approach for low-velocity impact on composite structures, Compos. Struct. 187 (March 2018) (2018) 71–84, http://dx.doi.org/10.1016/j.compstruct.2017.12.012.

[45] R. Bogenfeld, J. Kreikemeier, T. Wille, Validation of the low-velocity impact damage prediction through analytical scaling, Compos. Struct. 209 (November 2018) (2019) 715–726, http://dx.doi.org/10.1016/j.compstruct.2018.11.011, URL https://linkinghub.elsevier.com/retrieve/pii/S0263822318325583.

[46] D. Wilckens, R. Degenhardt, K. Rohwer, R. Zimmermann, M. Kepke, B. Hildebrandt, A. Zipfel, Cyclic buckling tests of pre-damaged CFRP stringer-stiffened panels, Int. J. Struct. Stab. Dyn. 10 (4) (2010) 827–851, http://dx.doi.org/10.1142/S0219455410003762.

[47] R. Khakimova, S.G. Castro, D. Wilckens, K. Rohwer, R. Degenhardt, Buckling of axially compressed CFRP cylinders with and without additional lateral load: Experimental and numerical investigation, Thin-Walled Struct. 119 (May) (2017) 178–189, http://dx.doi.org/10.1016/j.tws.2017.06.002.

[48] A.T. Nettles, L. Scharber, The influence of GI and GII on the compression after impact strength of carbon fiber/epoxy laminates, J. Compos. Mater. 52 (8) (2018) 991–1003, http://dx.doi.org/10.1177/0021998317719567.

[49] P. Paris, F. Erdogan, A critical analysis of crack propagation laws, J. Fluids Eng. 85 (4) (1963) 528–533, http://dx.doi.org/10.1115/1.3656900.

[50] R. Krueger, Development of a Benchmark Example for Delamination Fatigue Growth Prediction, Tech. rep., NASA, National Institute of Aerospace, HAmpton, Virginia, 2010, pp. 54–73.

[51] R. Bogenfeld, S. Freund, A. Schuster, An analytical damage tolerance method accounting for delamination in compression-loaded composites, Eng. Fail. Anal. 118 (Dec.) (2020) 104875, http://dx.doi.org/10.1016/j.engfailanal.2020.104875.